Pressure and velocity on an ogee spillway crest operating at high head ratio: experimental measurements and validation

Yann PELTIER, *University of Liege, ArGEnCo Department, Research Group on Hydraulics in Environmental and Civil Engineering (HECE), Allée de la Découverte, 13A, B52/3, 4000 Liege, Belgium*
Present affiliation: Laboratoire d'Hydraulique Saint-Venant (LHSV), Ecole des Ponts, CEREMA, EDF R&D, UPE, Chatou, France

Benjamin DEWALS, *University of Liege, ArGEnCo Department, Research Group on Hydraulics in Environmental and Civil Engineering (HECE), Allée de la Découverte, 13A, B52/3, 4000 Liege, Belgium*

Pierre ARCHAMBEAU, *University of Liege, ArGEnCo Department, Research Group on Hydraulics in Environmental and Civil Engineering (HECE), Allée de la Découverte, 13A, B52/3, 4000 Liege, Belgium*

Michel PIROTTON, *University of Liege, ArGEnCo Department, Research Group on Hydraulics in Environmental and Civil Engineering (HECE), Allée de la Découverte, 13A, B52/3, 4000 Liege, Belgium*

Sebastien ERPICUM, *University of Liege, ArGEnCo Department, Research Group on Hydraulics in Environmental and Civil Engineering (HECE), Allée de la Découverte, 13A, B52/3, 4000 Liege, Belgium. Author for correspondance: S.Erpicum@ulg.ac.be*

Pressure and velocity on an ogee spillway crest operating at high head ratio: experimental measurements and validation

ABSTRACT

This paper aims at validating pressure and velocity measurements conducted in two physical scale models of an ogee spillway crest operating at heads largely greater than the design head. The design head of the second model is 50% smaller than the one of the first model. No pier effect or air venting is considered in the study. The velocity field is measured by Bubbles Image Velocimetry. The relative pressure along the spillway crest is measured using pressure sensors. Comparison of measured velocities between both spillways indicates low scale effects, the scaled-profiles collapsing in most parts of the flow. By contrast, measurements of relative pressure along the spillway crest differ for large heads. A theoretical velocity profile based on potential flow theory and expressed in a curvilinear reference frame is fitted to the velocity measurements, considered as reference, for extrapolating the velocity at the spillway crest. Comparing the extrapolated velocity at the spillway crest and the velocity calculated from the relative pressure considering a potential flow finally emphasizes that bottom pressure amplitudes seem overestimated for the larger spillway, while an averaging effect might operate for the pressure measurements on the smaller spillway.

Keywords: ogee-crested weir, BIV, physical modeling, potential flow theory, pressure sensors, scale model.

1 INTRODUCTION

Uncontrolled ogee spillways are commonly used as flood release structures on dams. Their shape is designed regarding a given upstream head, the design head H_d, so that a zero relative pressure is obtained all along the crest profile (Hager 1987; USBR 1987) when the corresponding design discharge flows over the weir.

For at least thirty years and without considering potential effects of climate change, the availability of longer statistic chronicles and the evolution of the calculus methods impose a continuous review of the safety criteria of hydraulic structures (Millet et al. 1988; Xlyang & Cederström 2007). This usually results in an upward revision of the design floods for existing spillways. These spillways were indeed designed for smaller discharges/head as the ones requested by the revision, meaning some of these structures might face higher heads than the initial design head.

When considering ogee crest weirs, working with a higher head than the design one is not necessarily a drawback. The efficiency of the spillway, quantified by its discharge coefficient C_d, is indeed directly related to the pressure on the crest. For real upstream heads H smaller than the design head (head ratio H/H_d <1), the relative pressure on the crest is positive and the discharge coefficient decreases in comparison to its value for the design head. For head ratio higher than 1, the relative pressure on the crest is negative and the discharge coefficient increases. Under-designed ogee spillway crests (*i.e.* crest designed considering a design head smaller than the maximum operation head) are thus more efficient. Indeed, for a given upstream head, they enable to release a higher discharge than a spillway designed with a higher design head. However, negative relative pressure on the crest opens the door to flow detachment in case of connection of the lower part of the nappe with the atmosphere (for instance close to piers or at the end of short spillway chutes) or induces a risk of cavitation if the pressure falls locally below the water vaporization pressure (USACE 1990). This explains why ogee spillway crests are usually designed considering a design head equal to the maximum operation head. However, if enough care is taken regarding the pressure decrease effects, smaller design heads will provide higher discharge capacities.

In the literature, few studies focused on the flow characteristics over an ogee spillway crest for heads largely greater than the design head. Among the available references, very few studies deal with the flow dynamics and only the upstream head and the pressure along the weir-profile are generally measured. Rouse & Reid (1935) assessed the influence of the crest shape by comparing the discharge coefficients and the pressure distributions of three different ogee spillway profiles with those of a sharp crested weir until a head ratio, H/H_d, equal to three. Abecasis (1970) and Cassidy (1970) focused their investigations on a procedure to control the minimal pressure that occurs on an ogee spillway designed following the recommendations of USBR (1948) until a head ratio of three. Vermeyen (1992; 1991) studied, in the frame of a dam project, an ogee-spillway operation until a head ratio of five, but here again no information is available regarding the velocity distribution in the flow. After these previous studies, no more occurrences of studies dealing with ogee spillway working at high-head ratio can be found in the literature. The few studies we have found deal with other type of crests, e.g. round crest (Castro-Orgaz, 2008). The knowledge of the velocity field is yet paramount for better understanding the phenomena that drive the flow dynamics in the vicinity of the spillway and to validate the pressure measurements.

Within the framework depicted here-above, the study presented in this paper concerns the validation of velocity and pressure measurements conducted in 2 physical models with different scale factor of an ogee spillway crest operating at head ratios largely greater than one. In this study, no pier effect or air venting is considered. The experimental setup, the selected crest profile, the measurement

techniques and the theoretical background are presented in section 2. Then, the results are presented in section 3 and compared with theory in section 4 in order to be validated.

2 MATERIAL AND METHOD

2.1 Experimental facility

The main purpose of the project is to reproduce in a controlled environment flows over ogee spillways for heads much higher than the design head. To achieve this, high specific discharges are necessary. Due to the available discharge capacity in the laboratory and to the choice of a model 20 cm wide in order to minimize wall effects, a maximum design head of 15 cm was possible. Regarding real-life weirs, the dimensions of the present experiment roughly correspond to one tenth of prototypes.

In the present experiments, the use of a pressure chamber and of another fluid than water was not possible. Therefore, similarities in term of atmospheric pressure and surface tension could not be respected. The experimental facility was made of a large reservoir with an inner width of 0.90 m, a length of 4.00 m and a height of 3.20 m. At the extremity of the reservoir, a removable spillway with a vertical upstream face and a smooth chute was set (Figure 1). The chute was 4.5 m long in order to avoid any backwater effects on the flow in the vicinity of the crest.

The spillway profile being the key-parameter, geometric effects had to be minimized in order to obtain results as general as possible and independent from the scale of the experiment:

- Walls in polyvinyl chloride (PVC) were added in the reservoir for reducing the flow section to the width of the spillway: B = 0.20 m. The flow was thus confined in a 2D-vertical slice passing by the centreline of the spillway and contraction effects affecting the nappe stability were then avoided. The deformation of the new reservoir geometry was minimized by ensuring equality between the hydrostatic pressure distributions on both sides of the walls, through holes at the bottom of the PVC plates.
- Given the maximum design head of 0.15 m and the dimensions of the experimental facility, the expected maximum head over the spillway-crest, H_{max}, was found approximately equal to 0.75 m during the design phase. The independence of the spillway performance from the height of the upstream face of the spillway, h_{uf}, was ensured by setting h_{uf} equal to $3H_{max}$ (Melsheimer & Murphy 1970; Reese & Maynord 1987).

The feeding of the reservoir was performed in closed-loop, with one to three regulated pumps bringing the water through one to three pipes depending on the desired discharge. The pipes were terminated by a strainer, which allowed the injection of the water over the whole water column.

2.2 Spillway profiles

Two ogee spillways were constructed for this study. Their geometry follows the standards defined in the book "Hydraulic Design Criteria" (USACE 1987), *i.e.* the so-called "Waterways Experiment Station (WES) geometry", as also reported in USBR (1987). Consequently, the upstream quadrant is designed with 3 arcs of circle (see the coordinates in Table 1) and the downstream quadrant follows the power-law equation (1).

$$x^{1.85} = -2H_d^{0.85}z \quad (1)$$

where in the Cartesian coordinates system, x, y and z are the streamwise, spanwise and vertical directions respectively; $(x, y, z) = (0, 0, 0)$ at the crest. The z-axis is directed in the upward direction. The design head of the first spillway, W1, was set to 0.15 m, with a slope for the chute equal to 51°. The geometry of W2 was identical to W1, but a design head of 0.10 m was considered in order to be able to reach higher head ratios for the same discharges. This difference in scale was also used to identify the presence of possible scale-effects.

2.3 Measuring techniques

For each spillway, the flow dynamics were measured and analysed for five head-ratios, H/H_d, ranging from 1 to 5, by step of unity. The upstream head, the pressure along the spillway and the velocity field in the vicinity of the crest were measured.

2.3.1 Upstream head (water depth and discharge)

The upstream head, H, being one of the main parameters of the study, the measurement cross-section was chosen with care. It was positioned at a distance from the crest equal to at least twice the maximal head over the spillway, i.e. x_m = 1.5 m. At this distance, the feeding pipes and the spillway have low influences on the velocity profile in the reservoir, which is therefore quasi-uniform on the vertical. Under such flow conditions, the head was easily evaluated by measuring the water depth, h, relative to the crest of the spillway and by adding a term of kinetic energy calculated with the discharge velocity, V, equal to the ratio of the discharge, Q, to the area of the measurement cross-section (see Equation (2)).

$$H = h + \frac{V^2}{2g} = h + \frac{Q^2}{2gB^2\left(h + h_{uf}\right)^2} \quad (2)$$

The discharge was measured with an electromagnetic flowmeter (Siemens, MagFlow) mounted on each pipe. The uncertainty on the discharge, δQ, was equal to 0.7 L.s^{-1} with one pump, to 0.98 L.s^{-1} with two pumps and to 1.11 L.s^{-1} with three pumps.

The water depth was measured at $x = x_m$, using an ultrasonic probe (Microsonic, PICO+100). The precision on the measurement, δh, was estimated to ±1 mm by calibration tests.

2.3.2 Velocity fields

The velocity fields were obtained by means of Bubbles Image Velocimetry (BIV) (Bung & Valero 2016; Leandro et al. 2014; Ryu et al. 2005), which is a technique based on the classical PIV techniques, unless LED spotlights or natural light are used instead of laser and air bubbles are used as tracers.

Air-bubbles of approximately 5 mm in diameter were created at the reservoir bottom with a compressor and an injector. Given the velocity in the zone of interest, it was assumed that the bubbles have no relative motions compared to the ambient flow. The bubbles were lighted up using white lights focused above the spillway centreline. A high-speed video camera (Basler A504k) laterally positioned was used to record their displacements (Figure 2a). The exposure time of the camera was set to 500 µs with a sampling frequency of 400 Hz and the field of interest was saturated of light. These settings for the camera were chosen to:

- accurately capture air bubbles,
- minimize particle-motions on each frame,
- ensure a reasonable maximum displacement of pixels between two successive frames (max 20 pixels).

The frames of the resulting video-sequences were then extracted at the same sampling rate and each image was post-processed using ImageMagick (http://www.imagemagick.org), (Figure 2b-c). Each image was orthorectified and georeferenced, resulting in post-processed images in which one pixel was equal to a square of 1 mm × 1 mm. Finally, using a homemade PIV algorithm based on the one proposed by Hauet (2009) for Large-Scale PIV, the pixel displacements were assessed.

The PIV algorithm evaluates the maximum of likelihood between an interrogation area centred on a pixel on the first image and the same interrogation area centred for each pixel contained in a search area on the successive image. The subpixel precision is reached using a Gaussian fit (Hauet 2006).

The interrogation area in the first image is centred on the nodes of a mesh defined by the operator and was a square of 16 pixels × 16 pixels so as at least three or four bubbles were identifiable within this area. In order to limit the computation time, the search area was fixed for each flow-case and had therefore the same size for each node of the mesh. The search area was a square of at least 16 pixels × 16 pixels and at maximum 32 pixels × 32 pixels. The side length of the search area was evaluated for each flow-case and was chosen such as the velocity of a bubble crossing the search area between the first and the second image at the expected maximum velocity was measurable.

The mean velocity fields were then obtained from the averaging of 5,000 instantaneous velocity fields, with a theoretical uncertainty ranging between 6% and 17% (Hauet et al. 2008). Spurious vectors in the mean velocity fields were identified using a median filter (Westerweel & Scarano 2005) and were then simply removed.

2.3.3 Pressure

Eighteen relative pressure transducers (KELLER, PR23Y) with a measurement range between -5 m to +2 m in relative pressure were distributed along the centreline of the spillway on the weir crest. They gave 1 kHz measurements of the relative pressure through holes of 2 mm diameter perpendicular to the weir surface. The uncertainty of the pressure measurement was found equal to ±20 mm by calibration tests.

The positions of the sensors are displayed in Figure 4 (black circle). For the spillway W1, the sensors were regularly mounted along the spillway centreline with a spatial resolution close to 2 cm. By contrast for model W2, which was smaller than W1, the size of the sensors did not allow a regular positioning. As a consequence, the sensors were positioned as close as possible of the spillway-crest.

2.4 Theoretical profiles of velocity

Let us consider an elementary volume of fluid between two streamlines. The streamwise and normal directions are denoted by ξ and η respectively (Figure 3) in a curvilinear reference frame. With v being the norm of the velocity and θ indicating the local direction of the flow, the circulation around this element of volume is (Oertel 2010):

$$\Gamma = -\mathrm{d}\eta\,\mathrm{d}\xi\frac{\partial v}{\partial \eta} + \mathrm{d}\eta\,\mathrm{d}\xi\frac{\partial \theta}{\partial \xi}v \qquad (3)$$

If the flow is irrotational, the circulation around any volume is equal to zero and the velocities then derive from a field of potential $\phi(\xi,\eta)$. Under such conditions, the lines of isopotential are normal to

the velocity streamlines and at any point of the curvilinear reference frame, η (resp. ξ) is collinear (resp. normal) to an isopotential.

Let r be the signed radius of curvature of the streamline, *i.e.*:

$$r = \left(\frac{\partial \theta}{\partial \xi} \right)^{-1} \tag{4}$$

Equation (3) then reads:

$$\frac{\partial v}{\partial \eta} = \frac{v}{r} \tag{5}$$

The solution of this differential equation expresses the velocity profile along an isopotential, ϕ, as a function of the curvatures of the streamlines:

$$v(\eta) = v_0 \exp\left[\int_0^{\eta} \frac{\mathrm{d}s}{r(s)} \right], \quad v_0 = v(\eta = 0) \tag{6}$$

Considering a first-order Taylor series development of the function $r(\eta)$:

$$r(\eta) = r_0 + \left. \frac{\partial r}{\partial \eta} \right|_0 \eta, \quad r_0 = r(0) \tag{7}$$

Equation (6) finally writes:

$$v(\eta) = v_0 \left[1 - \frac{1}{r_0} \left. \frac{\partial r}{\partial \eta} \right|_0 \eta \right]^{\frac{-1}{\left. \frac{\partial r}{\partial \eta} \right|_0}} \tag{8}$$

The velocity profile described by Equation (8) depends on three parameters (v_0, r_0 and $\partial r/\partial \eta|_0$), which are used as tuning parameters in order to fit a theoretical velocity profile on the measurements. In our configuration, by setting $\eta = 0$ along the spillway crest, the curvature ($1/r_o$) can be easily calculated from the shape of the spillway, which is a particular streamline. Consequently, the number of tuning parameters reduces to two: v_0 = the velocity at the crest, $\partial r/\partial \eta|_0$ = the initial slope of the radius distribution at η = 0. This profile can then be fitted to experimental data taken along a given isopotential line.

The field of potential is computed using a regularised least-square method to solve an inverse problem, in which, $\boldsymbol{\phi}$, the vector of unknown potentials is found by solving in the least square sense the system $\mathbf{A}\boldsymbol{\phi} = (\boldsymbol{u},\boldsymbol{w})$, with $\mathbf{A}$ = gradient matrix expressed with a finite difference scheme. The resulting field of potential is finally linearly extrapolated, where velocity data were missing.

An additional result of the potential flow theory is that in an irrotational flow of Newtonian fluid, there are no head losses. As a consequence, the pressure in the flow can be deduced from the velocity using the Bernoulli's equation. The pressure P_{rel} at any elevation z is written as:

$$\frac{P_{rel}(x,z)}{\rho g} = H - z - \frac{u^2(x,z) + w^2(x,z)}{2g} = H - z - \frac{v^2}{2g} \qquad (9)$$

where H = upstream head, $u(x,z)$ and $w(x,z)$ = the longitudinal and vertical components of the local velocity respectively, v = the norm of the velocity, ρ = volume mass of water and g = the gravity acceleration.

3. RESULTS

3.1 Velocity

As illustrations of the BIV calculation, the velocity field for H/H_d = 5 is represented in Figure 4 for both spillways. The experimental facility being designed for the study of the flow dynamics at high head ratios, the measurements of the velocities are more accurate for flows above H/H_d = 2. Nevertheless, in all flow-cases no more than 9% of the measurements were considered as spurious and most of these vectors were located near the spillway crest, the chute bottom or close to the free surface, as highlighted by the velocity fields in Figure 4(a-b). These bad vectors were due to bad calculation of the BIV due to out of range pixel displacements on the video-sequences. With subpixel displacement or pixel displacements higher than 20 pixels, the BIV calculation is less accurate in finding the velocity. As previously mentioned, the spurious vectors were removed from the fields.

The rotation of the velocity field was then computed for every flow-case. It was found weak except at some points in the flow, mostly close to the spurious vector locations. We therefore considered that the condition of irrotational flow was fulfilled in most part of the flow, which emphasizes that Equation (8) should be a good approximation of the velocity evolution in the flow.

Thanks to the regularised least-square resolution previously described, the field of potential was computed and the velocity profiles along several isopotential lines were extracted from the velocity fields. The isopotentials are displayed in Figure 4(c) for three positions: x/H_d = -0.1, 0 and 0.5 along the spillway crest. The comparison of these lines for both spillway profiles in Figure 4(c) indicates that the scaled-isopotential lines collapse well in most parts of the flow. As a consequence, the scaled-velocities taken along these isopotentials can also be compared for both spillways (Figure 5). In Figure 5 it results that for each position, the scaled-velocity distributions of both spillways are well collapsing, which indicates that no scale effect can be identified. Nevertheless, the curvature of the velocity profile close to the spillway (lower part of the profile) is slightly different. For W1, the latter is stronger and the scaled-velocity close to the bottom seems to be higher than for W2, which could indicate an acceleration effect close to the spillway.

3.2 Pressure

The relative pressure measured along the spillway centreline is plotted in Figure 6. It is normalised by the upstream head. While for the unity head ratio, the relative pressure along the spillway is close to zero (to the uncertainty), for higher head ratios, the relative pressure strongly decreases with increasing head ratio. In all cases, the minimum of pressure is measured upstream from the crest at an abscissa belonging to [-0.25H_d – -0.23H_d], which is consistent with the literature (Melsheimer & Murphy 1970). The pressure then quickly increases to reach zero downstream from x = 1.5H_d except for the last section of W1. Nevertheless, a decrease of the relative pressure at this location is not consistent with what was observed during the experiments, the flow remaining attached to the spillway. This decrease of the relative pressure is mostly due to a systematic error of the sensor at this location. It is moreover not confirmed by measurements on W2.

Concerning the magnitude of the minimum relative pressure, similar behaviours are observed until H/H_d = 3 for W1 and W2, but for greater head ratio, measurements of W1 are systematically smaller (more intense pressure drop). This difference, which is coherent with the velocity measurements, could indicate a scale-effect, but can also be due to a measurement bias introduced by the size of the relative pressure sensor relatively to the size of the spillway. The surface of measurements is indeed larger for W2 than for W1, while it is clear that the minimal pressure is measured on a very limited length. Thus a larger surface averaging might occur in the case of W2.

4. DISCUSSION

As presented in the results' section, the velocity fields when scaled by the appropriate variable emphasise a good adequacy between both cases for head-ratios equal or greater than two. In contrast, the relative pressure measured along the spillway shows some discrepancies for head-ratios equal or greater than three. The full validation of the dataset therefore requires a method that puts into relation the pressure measurements and the velocity fields for both spillways.

For each spillway, a least square optimisation was performed on Equation (8) in order to find the best couple $\{v_0, \partial r/\partial \eta|_0\}$ to fit the experimental velocities (r_0 being fixed and deduced from the spillway geometry). As previously highlighted, the velocity profiles for both spillways being close at a given head-ratio (Figure 4(c)), an optimal mean fit per isopotential based on the data for both spillways can be found. In the sequel, by prolonging the fit until the coordinates η = 0 the corresponding velocity can be compared to the calculated velocity coming from the actual measurements of pressure assuming a potential flow.

The quality of the fit was first evaluated considering no uncertainties on the experimental data. The relative difference between the fit and the measurements is displayed for both spillways in Figure 7. Except for H/H_d=1, the mean fit and the experimental data are in good agreement, with differences between the theory and the experiments within ±5% in most part of the water column. The good adequacy between the fit and the data for W1 is highlighted in Figure 8, where the velocity profiles along three isopotentials are represented together with the mean fit. Similar results are obtained for W2 (not presented here)

The quality of the fit was then evaluated considering an uncertainty of ±17% on the experimental data (maximal uncertainty of the BIV technique). Keeping the curvature imposed by the spillway geometry, only v_0 = the velocity at the spillway surface and $\partial r/\partial \eta|_0$ = the initial slope of the radius distribution at $\eta = 0$ in Equation (8) will be affected by the change in the data. Comparisons between the original fit and the fits for 17 % greater or smaller velocity emphasize that uncertainty on the velocity only affects the amplitude of the velocity at the spillway. Moreover, the influence is not symmetrical. On one hand, if the velocity is underestimated by 17 %, v_0 is only affected by -2.9 %, on the other hand if the velocity is overestimated by 17%, v_0 is affected by 17%. By contrast, the initial slope of the radius distribution at $\eta = 0$ is not affected by a change in velocity magnitude. The good agreement of the fit and the experimental data therefore validates the use of Equation (8) and the extrapolation of the velocities towards $\eta = 0$. Nevertheless, one must keep in mind that the extrapolated velocity at the spillway surface has the same uncertainty as the experimental one.

The fit being validated, the measured relative pressure along the spillway crest can be converted into a velocity, v_{0p}, using Equation (9) and $z = z_{sensors}$. This velocity can then be compared to the fit of the velocity in $\eta = 0$ (*i.e.* v_0). In Table 2, the relative difference between v_0 and v_{0p} is given for each spillway (v_0 and v_{0p} are also reported in Figure 8, see markers at $\eta/H_d = 0$). In each case, the differences are in the range of uncertainty of the velocity. Nevertheless, trends appear between v_0 and v_{0p}. Except at H/H_d =1, when considering W1, the fit underestimates v_0 with increasing head-ratio, while it overestimates it for W2, the influence of H/H_d being less clear. These results are still difficult to interpreted, as two antagonist phenomena seem to interact at the spillway. For W1 the evolution of the relative difference indicates an overestimation of the relative pressure amplitudes by the pressure sensor, which is consistent with the higher velocities observed for W1 (see in Figure 5). By contrast, for W2, the amplitudes of the relative pressure are clearly underestimated where the minimum relative pressure was found, while it is well measured in the other sections. This confirms that a spatial averaging might operate for the measurements of the smallest relative pressure.

5. CONCLUSION

Velocity and pressure measurements on two identical ogee spillway crests at different scale (different design head) were conducted for heads largely greater than the design head. Velocity fields were found to be identical except very close to the spillway. Pressure evolution along the crest was found to be very similar for each model. However, for head ratio higher than 3, the lowest pressures, located just upstream of the crest, were significantly more important (smaller in absolute value) on the model with the larger design head.

Theoretical velocity profiles fitted on the experimental velocity data considering the potential flow theory have been used to extrapolate velocity amplitude at the spillway. On the other hand, velocity estimation at the crest has also been computed from measured pressures considering the same theoretical developments. Despite the differences between both estimations of the velocity at the spillway lie into the range of precision of the measurements, the comparison shows that the measured pressure drop seems overestimated for the model with the larger design head and underestimated for the one with the smaller design head. For the spillway with the smaller design head, this underestimation can be explained by an averaging effect due to the size of the sensor. No further scale effects affect the measurements.

6. ACKNOWLEDGMENTS

The authors are grateful for the physical model preparation by the laboratory technicians of HECE-ULg and the fruitful discussions about spillway flows with F. Stilmant (HECE-ULg), B. Blancher (EDF–CIH), J. Vermeulen (EDF–CIH) and D. Aelbrecht (EDF–CIH).

7. NOTATION

A gradient matrix expressed in finite differences (m^{-1})

B width of the spillway (m)

h water depth above the spillway-crest measured at $x = x_m$ (m)

δh uncertainty on the water depth (m)

h_{uf} height of the upstream face of the spillway (m)

g gravity acceleration ($m.s^{-2}$)

H head (m)

δH uncertainty on the head (m)

H_d design head (m)

H_{max} design maximal head (m)

P_{rel} relative pressure (m)

δP uncertainty on the pressure (m)

Q discharge at the inlet ($m^3.s^{-1}$)

δQ uncertainty on the discharge ($L.s^{-1}$)

r_0 curvature radius when $h_0 = 0$ (m)

r curvature radius (m)

r_0 curvature radius when $h_0 = 0$ (m)

u longitudinal component of the velocity ($m.s^{-1}$)

U discharge velocity ($m.s^{-1}$)

w vertical component of the velocity ($m.s^{-1}$)

v norm of the velocity ($m.s^{-1}$)

v_0 norm of the velocity in $\eta = 0$ ($m.s^{-1}$)

v_{0p} norm of the velocity in $\eta = 0$ computed from the relative pressure measured on the spillway ($m.s^{-1}$)

x streamwise direction (m)

x_m streamwise position of the measurement section (m)

y spanwise direction (m)

z vertical direction (m)

ξ curvilinear coordinate along a streamline (m)

η curvilinear coordinate along an isopotential line (m)

η_0 origine of the curvilinear coordinate along an isopotential line (m)

ϕ potential ($m^2.s^{-1}$)

θ local direction of the flow in the curvilinear reference frame (rad)

ρ volume mass of water ($kg.m^{-3}$)

REFERENCES

Abecasis, F.M., 1970. Discussion of "Designing Spillway Crests for High-Head Operation" by Cassidy. *Journal of the Hydraulics Division*, 96(12), pp.2654–2658.

Bung, D.B. & Valero, D., 2016. Optical flow estimation in aerated flows. *Journal of Hydraulic Research*, 54(5), pp.575–580.

Cassidy, J.J., 1970. Designing Spillway Crests for High-Head Operation. *Journal of the Hydraulics Division*, 96(3), pp.745–753.

Hager, W.H., 1987. Continuous Crest Profile for Standard Spillway. *Journal of Hydraulic Engineering*, 113(11), pp.1453–1457.

Hauet, A., 2009. Discharge estimate and velocity measurement in river using Large-Scale Particle Image Velocimetry [Estimation de débit et mesure de vitesse en rivière par Large-Scale Particle image Velocimetry]. *La Houille Blanche*, (1), pp.80–85.

Hauet, A., 2006. *Estimation de débit et mesure de vitesse en rivière par Large-Scale Particle Image Velocimetry*. Institut National Polytechnique de Grenoble - INPG.

Hauet, A. et al., 2008. Experimental System for Real-Time Discharge Estimation Using an Image-Based Method. *Journal of Hydrologic Engineering*, 13(2), pp.105–110.

Leandro, J., Bung, D.B. & Carvalho, R., 2014. Measuring void fraction and velocity fields of a stepped spillway for skimming flow using non-intrusive methods. *Exp Fluids*, 55(5).

Melsheimer, E.S. & Murphy, T.E., 1970. *Investigations of Various Shapes of the Upstream Quadrant of the Crest of a High Spillway*, Vicksburg, Missipi, USA: US Army Engineers Waterways Experiment Station.

Millet, J.C. et al., 1988. Augmentation De La Capacité Des Ouvrages D'évacuation De Divers Barrages. *Q63 R78, 16ème Congrès des Grands Barrages, San Francisco, USA*.

Oertel, H., 2010. *Prandtl-Essentials of Fluid Mechanics* 3rd ed., Springer New-York. Available at: http://link.springer.com/book/10.1007%2F978-1-4419-1564-1.

Reese, A.J. & Maynord, S.T., 1987. Design of Spillway Crests. *Journal of Hydraulic Engineering*, 113(4), pp.476–490.

Rouse, H. & Reid, L., 1935. Model Research on Spillway Crests. *Civil Engineering*, 5(1), pp.10–14.

Ryu, Y., Chang, K.-A. & Lim, H.-J., 2005. Use of bubble image velocimetry for measurement of plunging wave impinging on structure and associated greenwater. *Measurement Science and Technology*, 16(10), pp.1945–1953.

USACE, 1987. *Hydraulic Design Criteria* U. S. A. C. of Engineers, ed.,

USACE, 1990. *Hydraulic Design of Spillways* U. S. A. C. of Engineers, ed.,

USBR, 1987. *Design of Small Dams*, Denver, CO, USA: U.S. Department of Interior.

Vermeyen, T.B., 1991. *Hydraulic Model Study of Ritschard Dam Spillways*, Denver, CO, USA: U.S. Department of Interior. Available at: http://www.usbr.gov/pmts/hydraulics_lab/reportsdb/wrrl_reports_action2.cfm?id=R-91-08.

Vermeyen, T.B., 1992. Uncontrolled Ogee Crest Research. Available at: http://www.usbr.gov/pmts/hydraulics_lab/pubs/PAP/PAP-0609.pdf.

Westerweel, J.. & Scarano, F.., 2005. Universal outlier detection for PIV data. *Experiments in Fluids*, 39(6), pp.1096–1100.

Xlyang, J. & Cederström, M., 2007. Modification of Spillways for Higher Discharge Capacity. *Journal of Hydraulic Research*, 45(5), pp.701–709.

Table 1. Coordinates for upstream quadrant (USACE 1987).

x/Hd	0	-0.0500	-0.1000	-0.1500	-0.1750	-0.2000	-0.2200	-0.2400	-0.2600	-0.2760	-0.2780	-0.2800	-0.2818
z/Hd*	0	-0.0025	-0.0101	-0.0230	-0.0316	-0.0430	-0.0553	-0.0714	-0.0926	-0.1153	-0.1190	-0.1241	-0.1360

* The z-axis is oriented in the upward direction

Table 2. Relative difference in percent between v_0 and v_{0p}: $(v_0 - v_{0p})/v_{0p} \times 100$

	W1					W2				
H/H_d	1	2	3	4	5	1	2	3	4	5
x/H_d(min[*Prel*])	-14	5	6	-6	-9	-4	16	13	12	8
$x/H_d = 0$	-27	5	-2	-7	-11	-23	5	3	1	-2
x/H_d = 0.16-0.19	-17	6	-6	-12	-15	-24	5	4	5	4

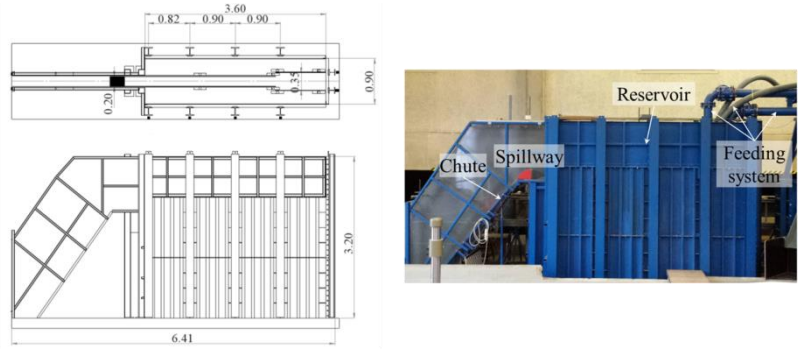

Figure 1. photograph, plan and section views of the experimental facility. Dimensions are in meter.

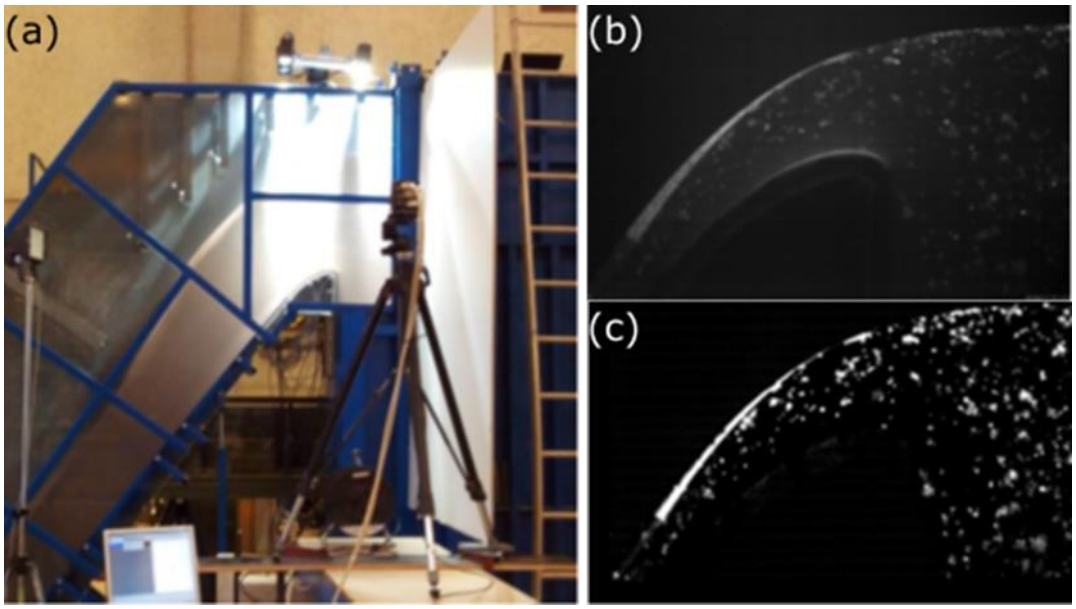

Figure 2. (a) BIV set-up. (b) Raw image. (c) Post-processed image.

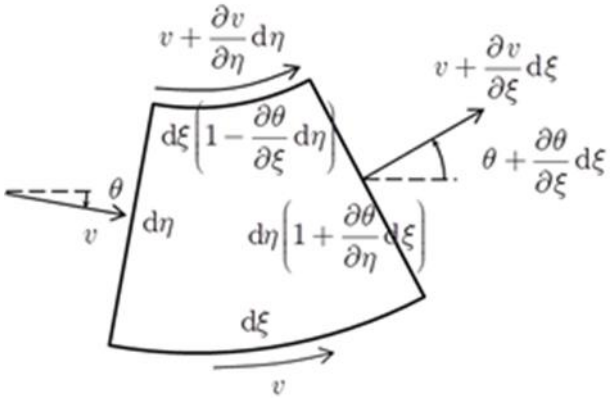

Figure 3. Element of volume between two streamlines

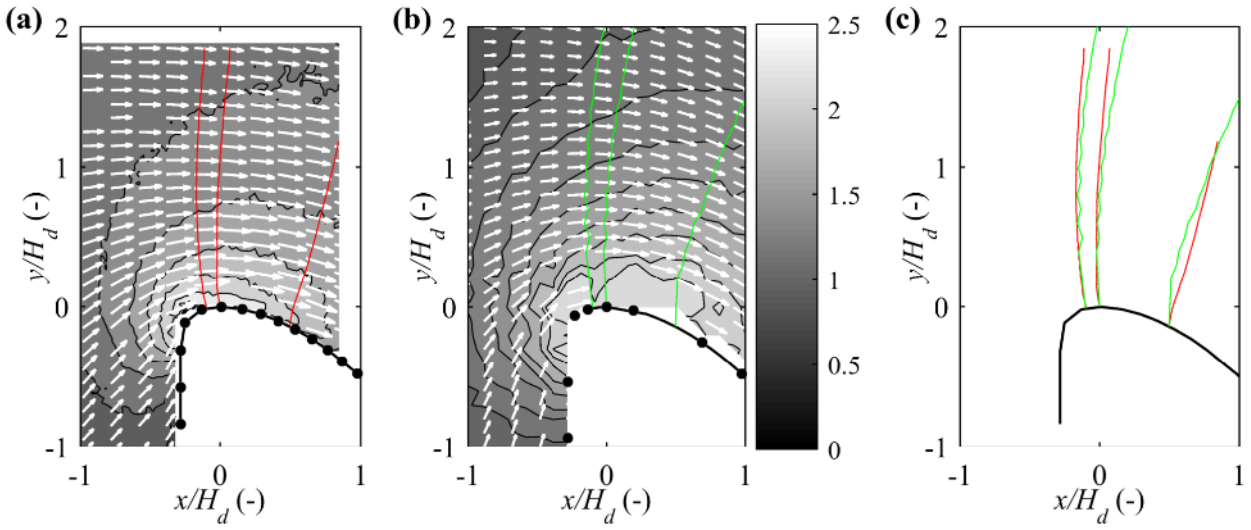

Figure 4. Contour plot of the norm of the velocity scaled by the discharge velocity V, velocity fields and isopotentials evaluated at three positions along the spillway crest (Black points = location of the pressure sensors). (a) W1, $H/H_d = 5$. (b) W2, $H/H_d = 5$. (c) Superimposition of the computed isopotentials of W1 and W2.

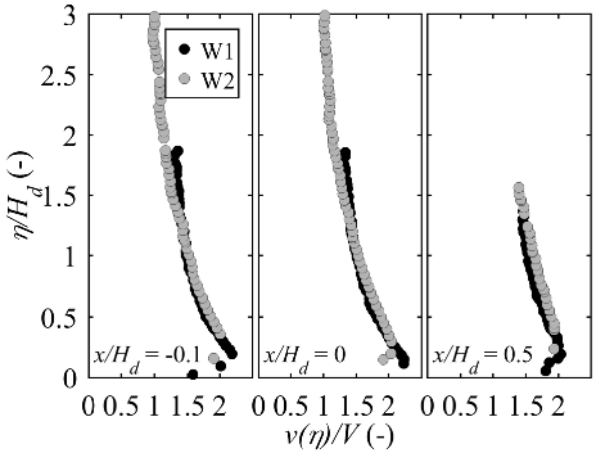

Figure 5. Distribution along the isopotentials displayed in Figure 4 of the velocity $v(\eta)$ normalized by the discharge velocity V.

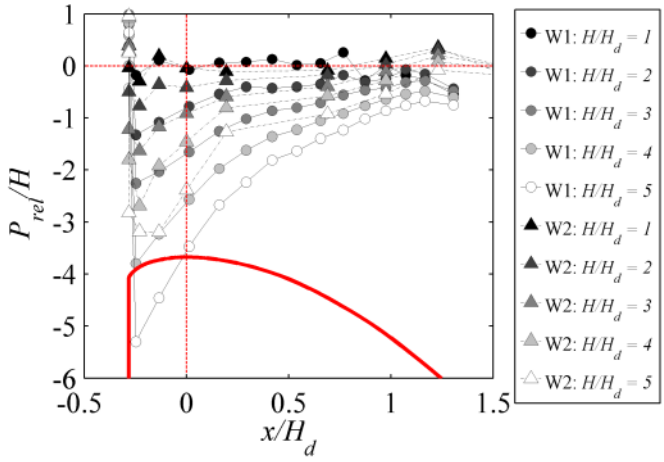

Figure 6. Relative pressure along the spillway crest

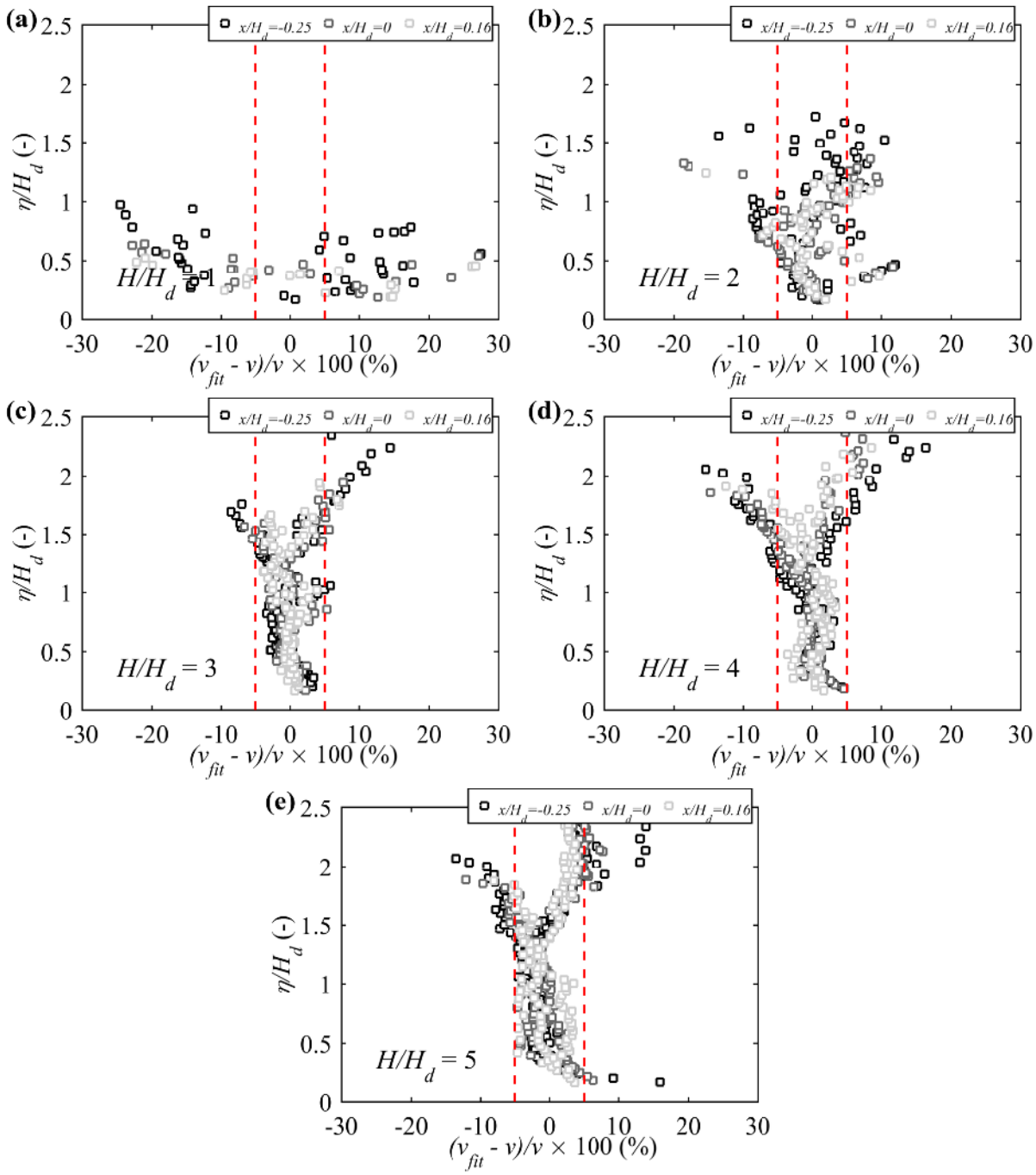

Figure 7. Comparison between the mean fit v_{fit} and the velocities v taken along three isopotentials corresponding to 3 measurement positions of relative pressure along the spillway. (a) $H/H_d = 1$, (b) $H/H_d = 2$, (c) $H/H_d = 3$, (d) $H/H_d = 4$ and (e) $H/H_d = 5$.

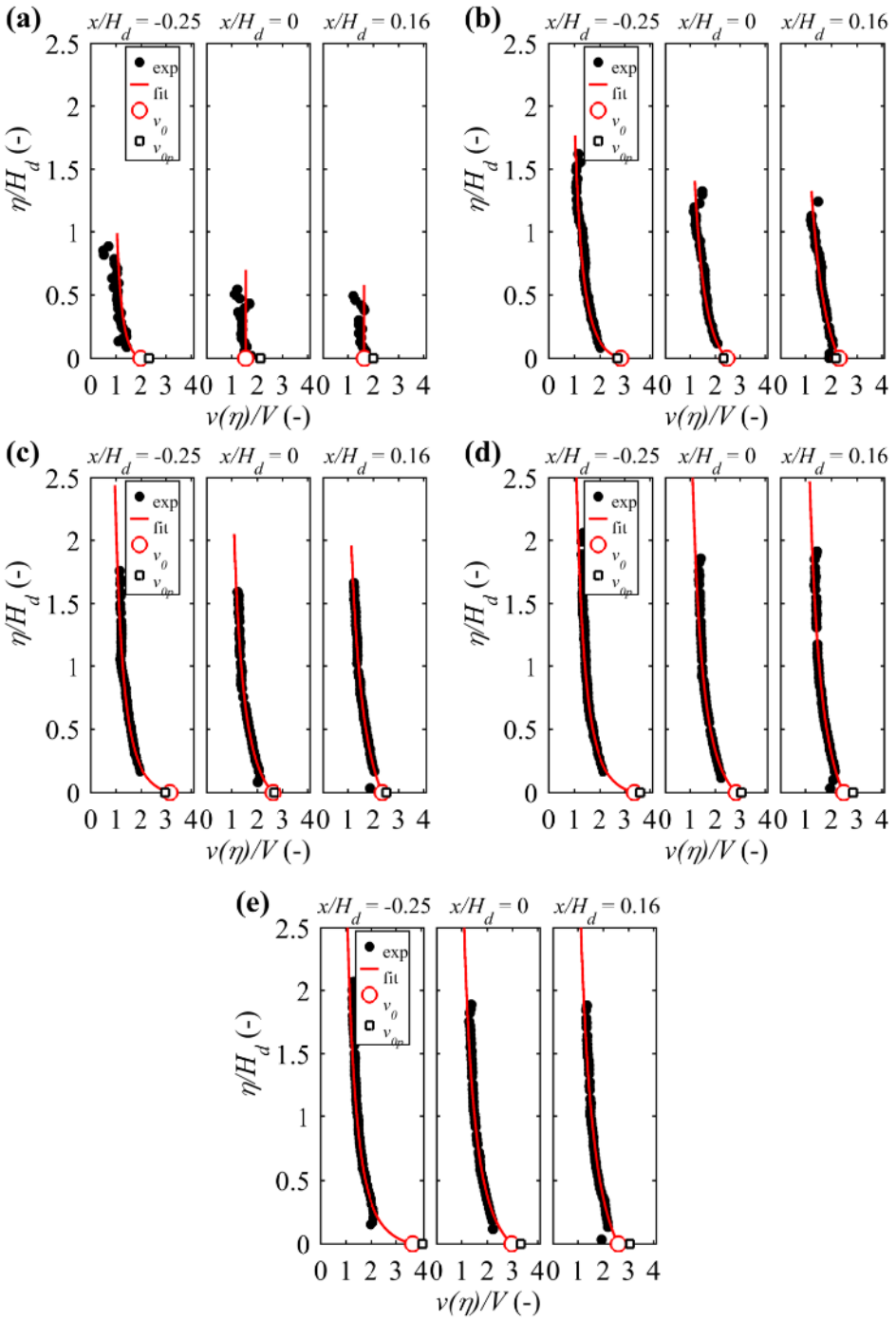

Figure 8. Fit of the velocities for W1 taken along three isopotentials corresponding to 3 measurement positions of relative pressure along the spillway. (a) H/H_d = 1, (b) H/H_d = 2, (c) H/H_d = 3, (d) H/H_d = 4, (e) H/H_d = 5.